Journal of Electron Spectroscopy and Related Phenomena 172 (2009) 21–26

Contents lists available at ScienceDirect

Journal of Electron Spectroscopy and Related Phenomena

journal homepage: www.elsevier.com/locate/elspec

Optimizing the PMIRRAS signal from a multilayer system and application to self-assembled monolayers in contact with liquids

M.W.A. Skoda[a,c,1], R.M.J. Jacobs[b], S. Zorn[c], F. Schreiber[c,*]

[a] Physical and Theoretical Chemistry Laboratory, South Parks Road, Oxford, OX1 3QZ, UK
[b] Chemistry Research Laboratory, Mansfield Road, Oxford, OX1 3TA, UK
[c] Institut für Angewandte Physik, Universität Tübingen, Auf der Morgenstelle 10, D-72076, Tübingen, Germany

ARTICLE INFO

Article history:
Available online 24 February 2009

Keywords:
Self-assembled monolayer
PMIRRAS
Water

ABSTRACT

Polarization modulation infrared reflection absorption spectroscopy (PMIRRAS) has become a powerful technique for the study of thin films on metal surfaces. We present a simple tool which allows the calculation and optimization of the PMIRRAS signal in multilayer systems. In order to illustrate the technique, an in situ experimental study of self-assembled monolayers on gold in contact with a μm thick water film is presented and the results compared with the calculation. A systematic series of measurements was performed on such a system and the signal intensity was recorded as a function of incident angle of the infrared beam. A strong, but broad peak in the signal-to-noise is observed at about 70° for an absorption peak at 1115 cm^{-1}, but its position strongly depends on the thickness of the water layer. This and other examples illustrate the importance of the calculations and simulations for the optimization of experimental parameters.

1. Introduction

The study of interfaces and interfacial phenomena in the field of bio and nano-science, especially of interfaces between artificial and biological media, is of tremendous importance [1,2]. The structure, formation and stability of self-assembled monolayers [3], which often serve as a bridge between artificial and biological systems, is also of great importance [4–10]. The study of topics such as the wetting properties of thin films [11], the "hydrophobic" interaction [12] and also biological systems at physiological conditions, usually requires the presence of aqueous media. A thorough investigation and a deeper understanding of effects at the molecular level can often only be gained by studying these systems in situ, in the physiological environment; this constitutes a challenge to the experimental methodology, since many characterization techniques have to be modified or do not work at all at these interfaces or through solution. Scattering techniques, such as neutron and X-ray scattering can serve as tools to obtain structural information of the whole system. However, when for instance information about molecular conformation is needed, spectroscopic techniques, such as X-ray photoelectron spectroscopy [13] or infrared spectroscopy have significant advantages. More recently, polarization modulation infrared reflection absorption spectroscopy (PMIRRAS) has been developed, a technique that, especially when employed in the reflection absorption geometry on metallic substrates, provides a high signal-to-noise ratio without the need for reference samples, as used in conventional infrared spectroscopy [14–16].

In situ PMIRRAS has been employed for studies at the water–air interface [17] and at the solid–liquid interface for electrochemical measurements [16,18]. Popenoe et al. [19] have described a method for the calculation of the mean square electric field in a stratified medium and have shown sample calculations for optimizing the FTIR signal. Similarly, Loring and Land [20] have described a method for the theoretical determination of parameters for optimum surface specificity in overlayer attenuated-total-reflection infrared spectroscopy. Here, we present a simple tool for the direct evaluation of the PMIRRAS signal generated by a multilayer system, with special emphasis on the situation of an organic monolayer (such as a SAM) on a metal film. The results can be analyzed as a function of angle of incidence and as a function of the thickness of one of the layers at a fixed angle of incidence. We demonstrate the functionality of this code by comparing calculations with experimental data for a model system. We also give some guidelines for the optimization of experimental conditions for other systems.

In a previous letter [21], we presented a PMIRRAS study of the influence of exposure of tri(ethylene glycol) (EG3)-terminated alkanethiol self-assembled monolayers to water. By means of PMIRRAS,

* Corresponding author.
E-mail addresses: maximilian.skoda@stfc.ac.uk (M.W.A. Skoda), frank.schreiber@uni-tuebingen.de (F. Schreiber).
[1] Present address: ISIS, STFC, Rutherford Appleton Laboratory, Didcot, OX11 0QX, UK.

0368-2048/$ – see front matter © 2009 Elsevier B.V. All rights reserved.
doi:10.1016/j.elspec.2009.02.005

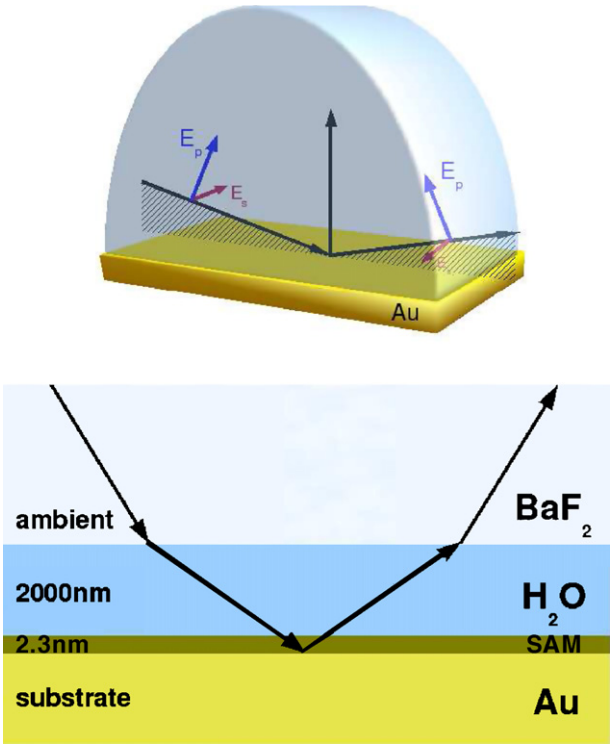

Fig. 1. Generic arrangement of layers used in the PMIRRAS calculation and experiments.

it was possible to observe in situ (i.e. in the presence of a water layer) subtle changes in the characteristic ether (C–O–C) vibrations originating from the region of the SAM that is in direct contact with the solvent. In this work a thin water layer was contained between the sample and a BaF_2 half-cylinder through which the observed spectra were collected. The half-cylinder was used to enable variation of the angle of incidence at the sample whilst keeping normal incidence at the air BaF_2 interface. This leads to the four-layer stack sketched in Fig. 1.

If in situ PMIRRAS measurements are performed on a multilayer system containing a variety of materials, for example the monolayers on a metallic substrate in contact with an aqueous solution described in our previous letter [21], the precise control of experimental parameters is required for a quantitative analysis. In particular, the thickness of the water layer between sample and BaF_2 prism, and the angle of incidence of the infrared light have to be optimized in order to obtain a good signal-to-noise ratio. In general, the signal-to-noise ratio in such experiments is lower compared to air measurements, owing to additional refractions and reflections at the prism–water and water–SAM interfaces, and also owing to absorption of the water layer itself. It was found that the signal-to-noise ratio in the wavelength region of the relevant peak varied strongly depending on the incident angle of the light and the liquid used (H_2O or D_2O). As the refractive indices of the materials involved in the optical setup vary with wavelength, and the Fresnel coefficients for a stack of optical layers vary with angle in a non-trivial way, it is not possible to predict the ideal conditions for the best signal-to-noise ratio for a given setup just by simple considerations. Therefore the Fresnel equations were implemented into the IgorPro [22] software for the purpose of determining the optimum experimental conditions. The formalism for the calculation of the reflectivity of the sample will be discussed in this section, and the experimental validation of the simulation will be given in the following section.

2. Simulation and optimization of the PMIRRAS signal

2.1. Mathematical framework and implementation

The propagation of electromagnetic waves through stratified media has been discussed in detail in the literature [23–25]. The present calculation uses the formalism and notation used by Hansen [26]. The basic implementation was obtained from Corn's group [27] and was extended to describe a four-layer system including s- and p-polarized light. From the resulting reflectivity for the whole stack, the PMIRRAS difference signal was computed (Eq. (1)) in order to compare these calculations with actual experimental data:

$$\frac{\Delta R}{R} = \frac{\Delta I_{sample}}{\langle I \rangle_{ref}} \approx \frac{I_p^{det} - I_s^{det}}{I_p^{det} + I_s^{det}} J_2(\phi_0) \tag{1}$$

where ΔI_{sample} is the measured signal, $\langle I \rangle_{ref}$ is the reference signal, $I_{s,p}^{det}$ are the recorded signals for p and s polarized light, respectively and $J_2(\phi_0)$ is the second order Bessel function. The detected PMIRRAS intensity depends on the cosine of the photoelastic modulator (PEM) phase ϕ. This phase in turn depends on the PEM frequency ω. The PMIRRAS signal containing a $\cos(\phi_0 \cos(\omega))$ term can then be expanded in terms of Bessel functions. Bessel functions of orders higher than two can usually be neglected. The Bessel function was thus not included in the calculation, since the experimental spectra can be corrected without major problems and the implicit Bessel function removed, for instance by manual baseline correction or subtraction of a reference spectrum. For an interesting discussion of some issues related to the signal generation of this type of modulation see, e.g. Ref. [28].

The formalism by Hansen is briefly described in the following section. The Fresnel equations can be re-written for the interface between two layers j and $j+1$ in the stack:

$$r_p^j = \frac{\hat{n}_{j+1}^2 \xi_j - \hat{n}_j^2 \xi_{j+1}}{\hat{n}_{j+1}^2 \xi_j + \hat{n}_j^2 \xi_{j+1}}, \quad t_p^j = \frac{2\hat{n}_{j+1}^2 \xi_j}{\hat{n}_{j+1}^2 \xi_j + \hat{n}_j^2 \xi_{j+1}} \tag{2}$$

$$r_s^j = \frac{\xi_j - \xi_{j+1}}{\xi_j + \xi_{j+1}}, \quad t_s^j = \frac{2\xi_j}{\xi_j + \xi_{j+1}} \tag{3}$$

where $\xi_j = \hat{n}_j \cos\theta_j = \sqrt{\epsilon_j - \epsilon_1 \sin^2(\theta_1)}$ and $\epsilon_j = \hat{n}_j^2$. Care has to be taken when calculating the square root of the complex expression for ξ, since the resulting hyperbolic functions are periodic and only the positive values of the real and imaginary parts must be used for the calculation. If the thickness of layer j is denoted by d_j and the complex variables

$$q_j = \frac{\xi_j}{\hat{n}^2} \quad \text{and} \quad \beta_j = \frac{2\pi d_j}{\lambda} \xi_j \tag{4}$$

are defined for convenience, then the optical matrices for layer j take the form for

Parallel (p) Polarization

$$M_j^p = \begin{pmatrix} \cos\beta_j & -\frac{i}{q_j}\sin\beta_j \\ -iq_j \sin\beta_j & \cos\beta_j \end{pmatrix} \tag{5}$$

Perpendicular (s) Polarization

$$M_j^s = \begin{pmatrix} \cos\beta_j & -\frac{i}{\xi_j}\sin\beta_j \\ -i\xi_j \sin\beta_j & \cos\beta_j \end{pmatrix} \tag{6}$$

In general for an N-layer system, $N-1$ matrices can be defined, since the ambient medium is semi-infinite. For the above-mentioned four-layer system, three matrices are needed. In order

to calculate the reflectivity of the whole stack, the characteristic matrix

$$M^{s,p} = \prod_{j=1}^{N-1} M_j^{s,p} = \begin{pmatrix} m_{11}^{s,p} & m_{12}^{s,p} \\ m_{21}^{s,p} & m_{22}^{s,p} \end{pmatrix} \tag{7}$$

has to be computed. Then the reflection coefficients for the whole stratified medium can be expressed using the following relations:

$$r_p = \frac{(m_{11}^p + m_{12}^p q_N)q_0 - (m_{21}^p + m_{22}^p q_N)}{(m_{11}^p + m_{12}^p q_N)q_0 + (m_{21}^p + m_{22}^p q_N)} \tag{8}$$

$$r_s = \frac{(m_{11}^s + m_{12}^s \xi_N)\xi_0 - (m_{21}^s + m_{22}^s \xi_N)}{(m_{11}^s + m_{12}^s \xi_N)\xi_0 + (m_{21}^s + m_{22}^s \xi_N)} \tag{9}$$

The reflection coefficients r_s and r_p for the entire stack are then used to compute the PMIRRAS signal r_{calc} (see also Eq. (1))

$$r_{calc}(\theta) = \frac{I_p - I_s}{I_p + I_s} \sim \left(\frac{\Delta R}{R}\right)_{exp} \tag{10}$$

The final signal is obtained by calculating the relative reflectance of the sample. This is given by the ratio of the reflectance of the stack with SAM to that without it:

$$I_{calc}(\theta) = \frac{r_{calc}^{SAM}}{r_{calc}^{noSAM}} \tag{11}$$

The IgorPro code plots r_s and r_p for the entire stack and the total PMIRRAS signal I_{calc}. The software can calculate these quantities as a function of angle for fixed thicknesses of SAM and water layer, or the signal can be evaluated at a given angle as a function of the thickness of either SAM or water layer. The resulting functions are very helpful for the determination of the ideal experimental conditions regarding optimum angle of incidence and the impact of the thickness of the water layer. In addition, the optical constants for H_2O and D_2O, which vary considerably in the mid-infrared region, can be automatically loaded from the tabulated values of Bertie et al. [29]. The refractive index of the BaF_2 half-cylinder is calculated using the following SELLMEIER approximation [30]:

$$n_{BaF_2}^2 = 1 + \frac{0.643356\lambda^2}{\lambda^2 - 0.057789^2} + \frac{0.506762\lambda^2}{\lambda^2 - 0.10968^2} + \frac{3.8261\lambda^2}{\lambda^2 - 46.3864^2} \tag{12}$$

This approximation is valid at 25 °C in the wavelength range of $\lambda = 265.2$–10346.5 nm (37707.4–966.5 cm^{-1}). The optical constants of gold were taken from [31].

2.2. Optimization of experimental parameters

Some examples are shown to illustrate the importance of the choice of incident angle and thickness of the water layer for the system which was investigated in our previous letter by using PMIRRAS. Samples presenting a hexa(ethylene glycol) (EG6OMe) terminated SAM were used as a model system in this study. The fingerprint region of a characteristic in situ spectrum, i.e. a spectrum taken through a thin (~ 1 μm) water layer, is shown in Fig. 2.

The typical shape of reflectivity curves for the present four-layer system is a smoothly rising curve with a broad peak at angles higher than 50°, which falls rather abruptly to zero at 90°. However, the position, width and relative height of the peak strongly depends on the thickness of the water layer sandwiched between barium fluoride half-cylinder and the sample. Whereas for relatively thin layers of H_2O, i.e. around 1000 nm, the peak is rather broad, centered at around 75°, the situation changes if the water layer becomes thicker (~ 3000 nm). Then the peak becomes much sharper and shifts towards lower angles. This means that

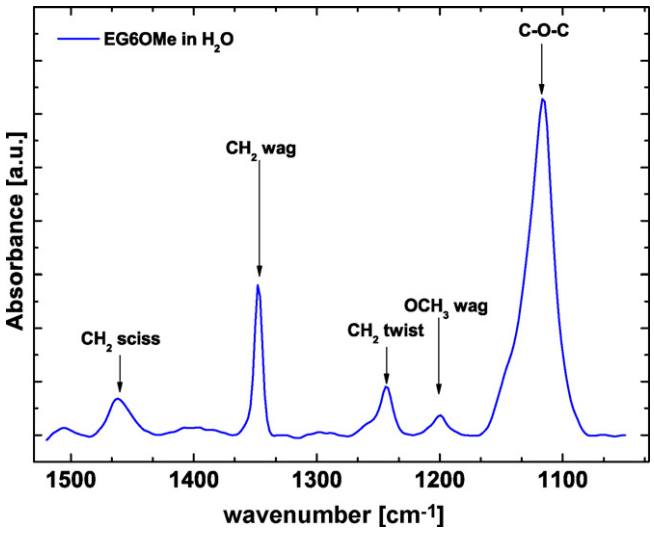

Fig. 2. Fingerprint region and peak assignments for an EG6OMe SAM taken in situ, in contact with a thin layer of H_2O.

the observed intensity of the IR absorption band (e.g. that of the C–O–C stretching vibration) can vary by a factor of up to seven between an angle of incidence of 80° compared to the optimum angle at 63° (Fig. 3 (a)). A more dramatic effect can be observed for D_2O in the CH stretching region. If absorption peaks in the CH region (around 2900 cm^{-1}) are measured, then a variation of the thickness from 1200 to 3200 nm can lead to a strong drop in the signal at angles away from the optimum angle at around 58°, as shown in Fig. 3(b). This behavior is caused by the difference in refractive index, which leads to total reflection between the BaF_2 half-cylinder and the water layer (the exact critical angle varies with wavelength). However, due to the relatively high imaginary part of the refractive index (equivalent to the absorption coefficient) for H_2O at 1115 cm^{-1}, the electromagnetic wave can still propagate into the water beyond the critical angle. In contrast, the absorption coefficient for D_2O at 2900 cm^{-1} is very small, and there is only the evanescent wave present at angles higher than the critical angle. Even in this case the intensity does not vanish immediately, since the evanescent field penetrates to depths of the order of the wavelength (i.e. a few micrometers) into the water.

Finally, the peak intensity can be plotted for a fixed angle as a function of the thickness of the water layer. An overview of the results is shown in Fig. 4. The absorption peak intensity drops strongly with the thickness of the water layer at angles much larger than the critical angle. The intensities do not drop very strongly for angles smaller than the critical one, and show an oscillatory behavior in the simulations. This is due to interference effects, when the thickness is of the order of the wavelength of the light. This effect is small even in the calculations, and it is not expected to be present in actual experiments due to roughness of half-cylinder and sample, and also due to potential misalignment (i.e. the water layer is not a slab of constant thickness, but has rather a wedged shape as a consequence of the inevitably imperfect mechanical assembly).

3. Comparison of calculations and experiments

In order to validate the simulations and compare them with experimental data, a systematic study of the angular dependence of the PMIRRAS was performed. With this setup it was possible to access angles between 40° and 90° using the liquid cell (Fig. 5).

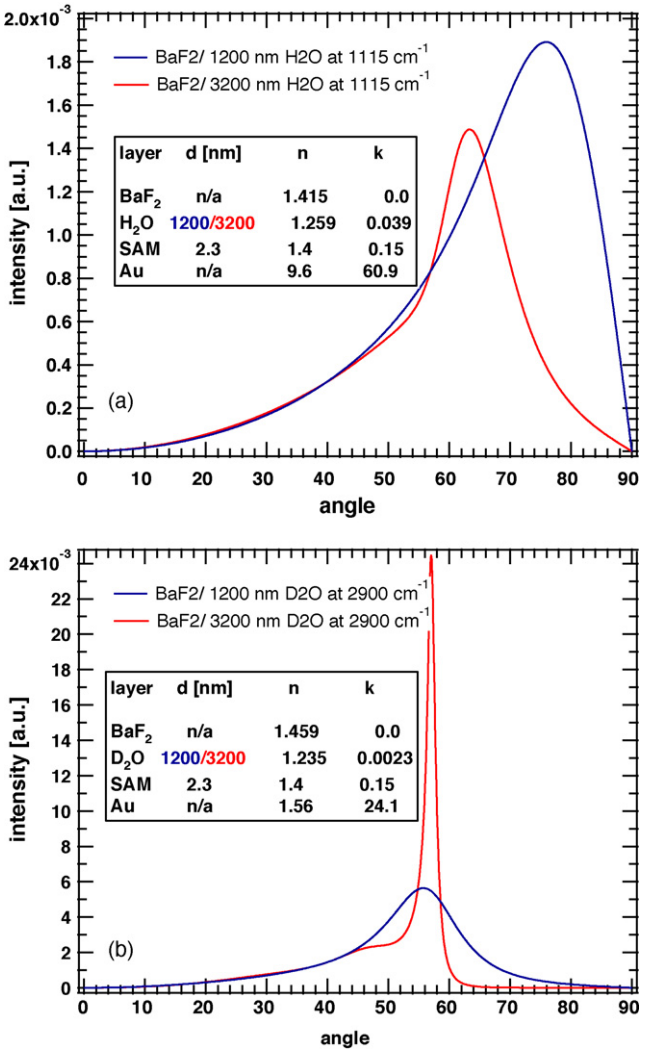

Fig. 3. (a) Simulation of the C–O–C peak intensity at 1115 cm^{-1} for a four-layer system consisting of barium fluoride, H_2O, monolayer and gold substrate (optical constants are shown in the inset). (b) Simulation of the C–H peak intensity at 2900 cm^{-1} for a four-layer system consisting of barium fluoride, D_2O, monolayer and gold substrate (optical constants are shown in the inset).The blue lines denote a water thickness of 1200 nm, while the red line represents 3200 nm of water. (For interpretation of the references to color in this figure legend, the reader is referred to the web version of the article.)

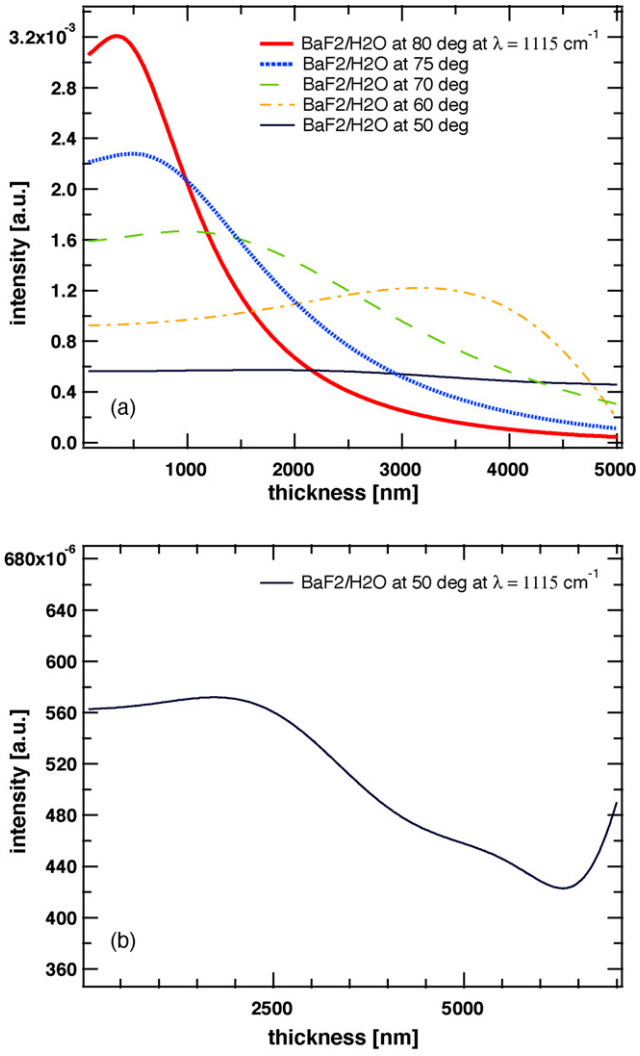

Fig. 4. (a) Simulation of the C–O–C peak intensity at 1115 cm^{-1} for a four-layer system consisting of barium fluoride, H_2O, monolayer and gold substrate for different, but fixed incident angles as a function of thickness of the water layer. (b) Detailed view of the plot for 50°.

3.1. Materials and methods

Prime grade wafers (Si-Mat, Germany) were coated with a 5 nm layer of chromium as an adhesion promoter and then with 100 nm of gold by thermal evaporation. Absolute ethanol purissimum pro analysi was purchased from Riedel-de Haën and used as-received. 1-Mercapto-11-undecyl hexa(ethylene glycol) was purchased from ProChimia, Poland, and was used as-received. Monolayers were obtained by self-assembly from a 0.5 mM solution of the thiol in ethanol. The immersion time for self-assembly was approximately 20 h.

A BaF_2 half-cylinder was employed to allow normal incidence with respect to the surface normal of the half-cylinder at any incident angle (Fig. 5). The BaF_2 half-cylinder had a radius of 2.5 cm and a height of 3 cm, resulting in a flat rectangular area of 3 cm × 5 cm which was facing the sample. The half-cylinder was designed to rest on a Viton seal along the outer edges of the rectangular surface, allowing the trough underneath it to be filled with the desired liquid using the in- and outlet nozzles. However, in the case of aqueous solutions it was sufficient to place a drop of the solution on the sample and press the sample gently against the half-cylinder. The surface tension was enough to keep the sample attached and prevent fast evaporation. The half-cylinder was fastened with a metal clamp from the top of the round surface, which rested on a curved PTFE block, thereby distributing the pressure evenly onto the half-

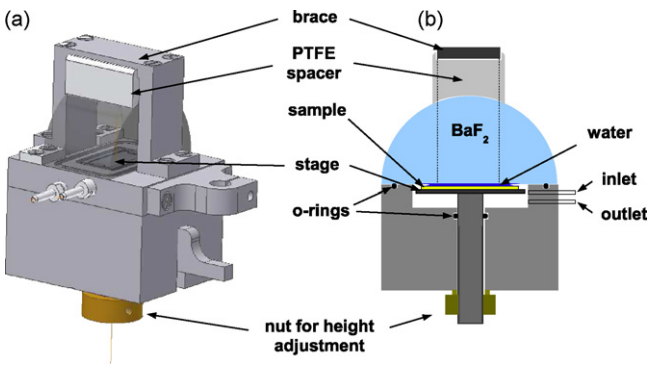

Fig. 5. Sketch of the cell used for in situ PMIRRAS measurements. (a) Drawing including BaF_2 equilateral prism (courtesy of A. Treftz). (b) Side view.

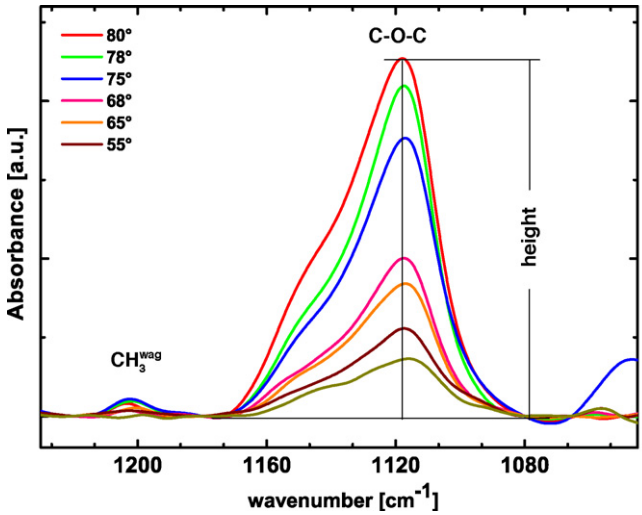

Fig. 6. Measured C–O–C peak heights for various angles on an EG6OMe coated SAM in air.

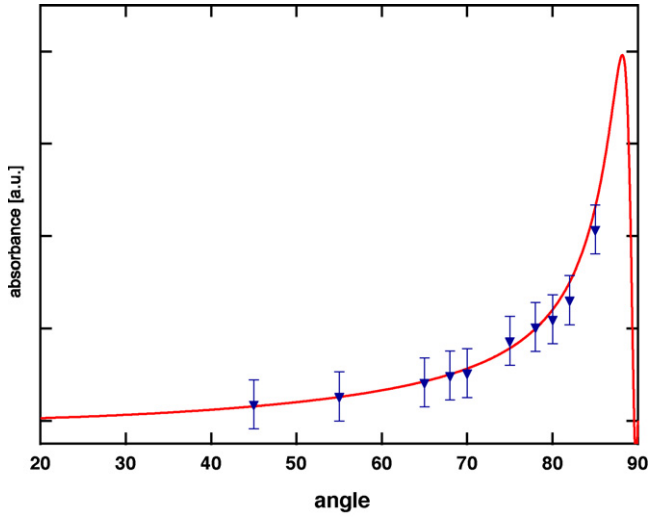

Fig. 7. Comparison of calculated (solid red line) and measured (blue triangles) reflectivities for various angles of the characteristic C–O–C absorption band of an EG6OMe coated SAM in air. The calculation was performed at 1118 cm^{-1}.

cylinder. The sample rested on a sample stage of 2.5 cm × 3 cm which could be moved vertically by hand, using a fine thread. The appropriate thickness of a few micrometers of the liquid layer was achieved by adjusting the pressure of the sample stage against the half-cylinder. Because the thickness of the water layer was required to be around 1 μm, it was not possible to use a spacer or to adjust the thickness reproducibly to the exact same value. Instead, the thickness of the water layer was determined by ellipsometry measurements on a Beaglehole instrument before and after the PMIRRAS measurement, as described in our previous letter [21].

Spectra were taken using a dry-air-purged Bio-Rad FTS-6000 Fourier transform IR spectrometer with polarization modulation unit. Data were collected at 20 Hz at a resolution of 8 cm^{-1}, and an under-sampling ratio (UDR) of 4 was used to improve the speed of data acquisition. To avoid aliasing, we placed a UDR filter into the optical path of the IR beam, which prevents radiation at higher wavenumbers from reaching the detector. A polarization modulator (PM) was employed, which was controlled by a Hinds Instruments PEM-90 photoelastic modulator control unit. The half-wave retardation was set at 37 kHz. The sample was placed vertically between a focusing mirror and a ZnSe lens in front of the detector. Complementary spectra were taken with a Bruker VERTEX 70 spectrometer.

First, the sample was measured at incident angles ranging from 45° to 85° with respect to the surface normal of the sample. Because the measured PMIRRAS spectra still contained a second order Bessel function, as described above, they had to be baseline-corrected in order to obtain the true spectrum (the same correction procedure was employed for all samples). A set of seven points at positions 1260, 1220, 1180, 1080, 1065, 1050 and 1030 cm^{-1} was used for all samples to interpolate the shape of the baseline. The interpolation points were chosen to lie well away from the peak of interest in the spectrum. This standard correction procedure was necessary for the determination of the peak intensity for different samples, especially for the in situ measurements, where the whole angle series could not be measured without refilling the liquid cell. The liquid had to be replaced after about 1 h due to partial drying or air bubble formation.

3.2. EG6OMe SAM in contact with H_2O

The EG6OMe sample was measured in air (Fig. 6). The peak heights were determined and compared to the calculated values. The measured values were only multiplied by a constant factor to account for the efficiency of the optics in the experimental setup. As can be seen from Fig. 7, the measured values are in excellent agreement with the calculated curve. The data points at angles higher than about 80° are slightly lower than the calculated curve. This can be explained by the large size of the footprint of the beam compared to the sample at grazing angles, as was verified in measurements with differently sized samples. If the sample is sufficiently long in the direction of the beam, then the overspill can be minimized or even eliminated and the data points are commensurate with the calculated values. The peak heights were taken to be the vertical distance between the abscissa of the corrected spectra and the highest point of the C–O–C peak at about 1118 cm^{-1} (Fig. 6). The error was estimated by repeated measurements of one sample at one given angle at different times and calculating the standard deviation of the measured values.

A second series of measurements was performed in situ, using the liquid cell, where the EG6OMe SAM was in contact with a thin layer of water. Because the solubility of BaF_2 is about 1.6 g/kg in water at room temperature [32], a 0.1 M NaF/water solution was used instead in order to avoid damage to the BaF_2 half-cylinder as a consequence of prolonged exposure to water. The duration of one in situ measurement at a resolution of 8 cm^{-1} was about 20 min including the time required for the calibration of the instrument after the angle was changed.

The results of the angle dependent measurements and the calculation are compared in Fig. 8. The optical constants used for the four-layer model are listed in Table 1. Establishing the systematic error for the in situ measurements was more difficult than for the data taken in air. The data point at 80° was taken nine times under similar conditions and the standard deviation of these measurements was taken as error estimate for all other data points, most of which were measured only once. Despite the large error bars, the experimental data reproduce well the trend of the calculation. In the simulation only one overall scaling factor was used between experimental and calculated data points; no other fitting param-

Table 1
Optical constants for the PMIRRAS calculation in Fig. 8.

Layer	*d* (nm)	*n*	*k*
BaF_2	n/a	1.4148	0.0
H_2O	1200	1.2588	0.03922
SAM	2.8	1.4	0.14
Au	n/a	9.38	60.08

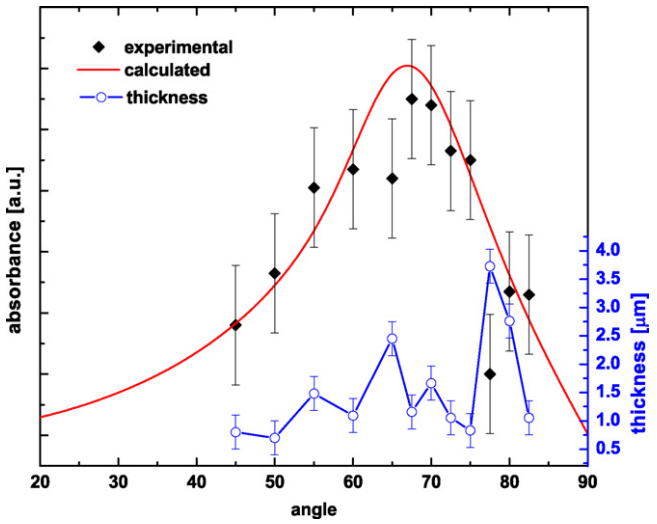

Fig. 8. Comparison of calculated (red solid line) (at 1118 cm^{-1}) and measured (black diamonds) reflectivities for various angles of the characteristic C–O–C absorption band of an EG6OMe coated SAM in a 0.1 M H_2O/NaF solution. The red line is the PMIRRAS calculation for a four-layer stack with optical constants listed in Table 1 at 1118 cm^{-1}. The blue solid line with open circles denotes the actual measured thickness of the water layer for each angle. (For interpretation of the references to color in this figure legend, the reader is referred to the web version of the article.)

eters were used. The additional line in Fig. 8 shows the measured water layer thickness for each point. The reason for the larger discrepancy at 65° and 77.5° is the fact that the actual thickness of the water layer was much larger than the thickness used for the calculation of all angles.

In addition, during the experiments it was noticed that, under certain conditions, for instance when the sample is not entirely parallel to the barium fluoride prism, thickness measured by the relatively small laser spot (ca. 1 mm × 2 mm), may vary from the actual range of thicknesses over which the much larger beam of infrared light is averaging (ca. 0.5 cm × 3 cm).

4. Conclusions

To conclude, this study demonstrates the importance of choosing and controlling the experimental parameters (incident angle, thickness of the water layer, sample size, etc.), in particular for in situ PMIRRAS experiments. The presented software can serve as an aid for the selection of the optimum settings regarding angle of incidence and thickness of the liquid layer when a complex multilayer system is studied, especially if the optical constants of the employed materials strongly depend on wavelength. The accuracy of the calculated data was examined by a systematic experimental study and was found to be in excellent agreement with the experimental values.

Acknowledgement

This work was supported by the Engineering and Physical Sciences Research Council (EPSRC).

References

[1] E.A. Vogler, J. Biomater. Sci. Polym. Ed. 10 (1999) 1015–1045.
[2] P. Ball, Nature 423 (2003) 25–26.
[3] F. Schreiber, J. Phys.: Condens. Matter 16 (2004) R881–R900.
[4] C.D. Bain, G.M. Whitesides, Angew. Chem. 28 (4) (1989) 506–512.
[5] A. Ulman, Chem. Rev. 96 (4) (1996) 1533–1554.
[6] F. Schreiber, Prog. Surf. Sci. 65 (2000) 151–257.
[7] J. Love, L. Estroff, J. Kriebel, R. Nuzzo, G. Whitesides, Chem. Rev. 105 (4) (2005) 1103–1170.
[8] L. Becucci, R. Guidelli, Q. Liu, R. Bushby, S. Evans, J. Phys. Chem. B 106 (40) (2002) 10410–10416.
[9] A. Erbe, R. Bushby, S. Evans, L. Jeuken, J. Phys. Chem. B 111 (13) (2007) 3515–3524.
[10] R. Madueno, M.T. Raisanen, C. Silien, M. Buck, Nature 454 (7204) (2008) 618–621.
[11] I. Engquist, I. Lundstroem, B. Liedberg, J. Phys. Chem. 99 (32) (1995) 12257–12267.
[12] D. Chandler, Nature 437 (2005) 640–647.
[13] Y. Zubavichus, M. Zharnikov, Y. Yang, O. Fuchs, E. Umbach, C. Heske, A. Ulman, M. Grunze, Langmuir 20 (25) (2004) 11022–11029.
[14] T. Buffeteau, B. Desbat, J.M. Turlet, Appl. Spectrosc. 45 (3) (1991) 380–389.
[15] I. Zawisza, X. Cai, V. Zamlynny, I. Burgess, J. Majewski, G. Szymanski, J. Lipkowski, Pol. J. Chem. 78 (2004) 1165–1181.
[16] V. Zamlynny, I. Zawisza, J. Lipkowski, Langmuir 19 (1) (2003) 132–145.
[17] D. Blaudez, T. Buffeteau, J. Cornut, B. Desbat, N. Escafre, M. Pezolet, J. Turlet, Appl. Spectrosc. 47 (6) (1993) 869–874.
[18] C. Methivier, B. Beccard, C. Pradier, Langmuir 19 (21) (2003) 8807–8812.
[19] D.D. Popenoe, S.M. Stole, M.D. Porter, Appl. Spectrosc. 46 (1992) 79–87.
[20] J.S. Loring, D.P. Land, Appl. Opt. 37 (16) (1998) 3515–3526.
[21] M. Skoda, R. Jacobs, J. Willis, F. Schreiber, Langmuir 23 (3) (2007) 970–974.
[22] IgorPro 5 - Wavemetrics Inc., http://www.wavemetrics.com/, 2005.
[23] M. Born, E. Wolf, Principles of Optics: Electromagnetic Theory of Propagation, Interference and Diffraction of Light, 6th ed., Cambridge University Press, 1997.
[24] F. Abelés, Ann. Phys. 5 (1950) 596.
[25] F. Abelés, Advanced Optical Techniques, John Wiley & Sons, New York, 1967.
[26] W. Hansen, J. Opt. Soc. Am. 58 (1968) 380–390.
[27] R.M. Corn, http://corninfo.ps.uci.edu/writings/Ref4txt.html.
[28] C.G. Hu, L.D. Sun, Y.N. Li, M. Hohage, J.M. Flores-Camacho, X.T. Hu, P. Zeppenfeld, J. Opt. Soc. Am. A 25 (6) (2008) 1240–1245.
[29] J.E. Bertie, M.K. Ahmed, H.H. Eysel, J. Phys. Chem. 93 (1989) 2210–2218.
[30] I.H. Malitson, J. Opt. Soc. Am. 54 (1964) 628.
[31] E.D. Palik (Ed.), Handbook of Optical Constants, Academic Press Inc., 1985.
[32] D.P. Lide (Ed.), CRC Handbook of Chemistry and Physics, 87th ed., CRC Press, http://www.hbcpnetbase.com, 2006.